Development and Characterization of Low-Density Ca-Based Bulk Metallic Glasses: An Overview

O.N. SENKOV, D.B. MIRACLE, V. KEPPENS, and P.K. LIAW

Ca-based bulk metallic glasses (BMGs) have unique properties and represent a new seventh group of BMGs. Many of them have excellent GFA, which can be related to their efficient atomic packing, low onset driving force for crystallization, and high viscosity (high relaxation time) of the supercooled liquid. The Ca-based glasses have the lowest density and elastic moduli among all BMGs discovered to date. Unfortunately, as many other glasses, Ca-based BMGs are brittle below the glass transition temperature, and they also have marginal oxidation and corrosion resistance. The latter can be improved by proper selection of alloying elements. In this article, we review recent work on the development of low-density Ca-based BMGs and discuss the effect of alloy composition on the thermal, physical, and chemical properties of these glasses.

DOI: 10.1007/s11661-007-9334-z

I. INTRODUCTION: CLASSIFICATION AND MAIN FEATURES OF Ca-BASED BULK METALLIC GLASSES

NEW metallic alloys with exceptional glass forming ability (GFA), which can remain amorphous after solidification at relatively low cooling rates typical of conventional metal mold casting, open new opportunities both for fundamental studies and technological advances. High thermal stability, exceptional mechanical and physical properties, as well as the ability to be plastically formed in the supercooled liquid state make bulk metallic glasses (BMGs) attractive for engineering applications. Over the last two decades, a number of BMGs based on Pd, Zr, rare earth metals, Fe, Cu, Ni, Mg, and some other elements have been produced, and different methods have been proposed to guide the discovery of new glasses with better GFA.[1–4]

The Ca-based BMGs are a relatively new class of amorphous alloys. The first Ca-based BMGs were reported by Amiya and Inoue in 2002.[5,6] They produced two ternary glasses, $Ca_{57}Mg_{19}Cu_{24}$ and $Ca_{60}Mg_{20}Ag_{20}$, with a maximum diameter of 4 mm and a quaternary $Ca_{60}Mg_{20}Ag_{10}Cu_{10}$ with a maximum diameter of 7 mm. During the following years, a number of Ca-Mg-Zn, Ca-Mg-Cu, Ca-Mg-Al, Ca-Al-Cu, Ca-Mg-Zn-Cu, Ca-Mg-Al-Zn, Ca-Mg-Al-Cu, Ca-Y-Mg-Cu, Ca-Mg-Al-Zn-Cu, Ca-Y-Mg-Zn-Cu, and Ca-Mg-Al-Ag-Cu BMGs with thicknesses up to 10 mm were reported by Senkov *et al.*[4,7–12] Approximately, at the same time, Park and Kim[13] produced a $Ca_{65}Mg_{15}Zn_{20}$ alloy, which was fully amorphous in up to 15-mm diameter cross sections. They also developed several other Ca-Mg-Zn amorphous alloys.[14] Guo *et al.*[15] reported on Ca-Al-Cu, Ca-Al-Ag, and Ca-Al-Mg amorphous alloys with a maximum diameter of 2 mm and Ca-Mg-Al-Cu and Ca-Mg-Al-Ag glasses with a maximum diameter of 4 mm. All of these Ca-based BMGs can be described by the formula[4,7]

$$Ca_A(Y,Ln)_B(Mg,Sn)_C(Al,Ag,Ga,Zn)_D(Cu,Ni)_E \quad [1]$$

with $A = 40$ to 70, $B = 0$ to 30, $C = 0$ to 30, $D = 0$ to 35, $E = 0$ to 35, and $A + B + C + D + E = 100$.

A strong topological basis[4,16–20] exists for the compositions represented in Eq. [1], and a structural model has recently been developed following these background developments.[21] The breadth of Eq. [1] and the results just cited indicate that many Ca-based alloys are good glass formers. A graphical presentation of Eq. [1] is shown in Figure 1, where concentrations of the elements are plotted *vs* their atomic radius ratios R_i (*i.e.*, the atomic radius of an element divided by the atomic radius of Ca). The elements with the same R_i (within ±2 pct deviation) are combined in the same group, and their sum concentration range is shown as solid bars. It can be seen from Figure 1 that R_i has discrete values, which correspond to densely packed solute-centered clusters with solvent atom coordination numbers of 8, 9, 10, and 12 at $R_i = 0.62$, 0.71, 0.80, and 0.90, respectively,[17] and the elements in each group have specific concentration ranges, which are necessary for efficient atomic packing.[10,16,21,22] Such atomic-concentration arrangement of the alloying elements in the Ca-based BMGs, which provides efficient atomic cluster packing,[17,22] may be one of the reasons for their good GFA.

O.N. SENKOV, Senior Scientist, is with UES, Inc., Dayton, OH 45432. Contact e-mail: oleg.senkov@wpafb.af.mil D.B. MIRACLE, Senior Scientist, is with the Air Force Research Laboratory, Materials and Manufacturing Directorate, Wright-Patterson AFB, OH 45433. V. KEPPENS, Associate Professor, and P.K. LIAW, Professor, are with the Department of Materials Science and Engineering, The University of Tennessee, Knoxville, TN 37996, USA.

This article is based on a presentation given in the symposium entitled "Bulk Metallic Glasses IV," which occurred February 25–March 1, 2007 during the TMS Annual Meeting in Orlando, Florida under the auspices of the TMS/ASM Mechanical Behavior of Materials Committee.

Article published online October 19, 2007

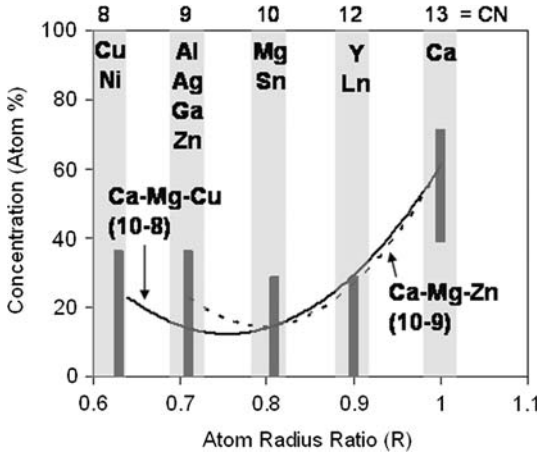

Fig. 1—Atomic size ratio *vs* concentration of elements in Ca-based BMGs. Atomic size distribution plots for two ternary alloys, Ca-Mg-Zn (dotted line) and Ca-Mg-Cu (solid line), and their structural designations[10,21] are also shown here. Typically, no more than three of the four possible solute sizes are present in any given metallic glass.

Recently, Takeuchi and Inoue conducted a classification of BMGs.[23] According to their classification, which is shown in Figure 2, Ca-based glasses represent a new seventh group of BMGs, which consists of simple alkaline metals (Ca and Mg) and late transition metals (*e.g.*, Ag, Cu, Zn, and Ni). However, it is well established now and represented by Eq. [1] that Ca-based BMGs may also contain Al-, Ga-, Y-, and Ln-group metals. Therefore, the diagram in Figure 2 should be modified by adding two arrows, which add these elements to the seventh group.

The Ca-based metallic glasses have unique properties. First, they are built on one or two simple metals, Ca and Mg, while all other BMGs are transition-metal–based alloys (Figure 2). Second, Ca-based amorphous alloys

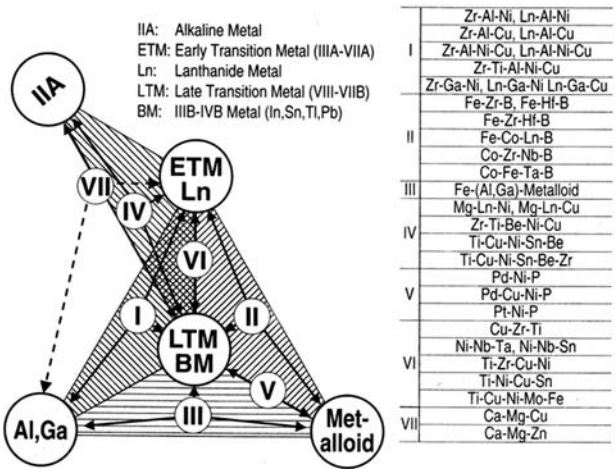

Fig. 2—Classification of BMGs by Takeuchi and Inoue.[23] The Ca-based glasses, in accordance with Eq. [1], may also contain Al, Ga, Y, and lanthanide metals. Therefore, the seventh group should be expanded to include these elements, as indicated by dashed arrows in this figure.

have very good GFA, and even their ternary alloys can have a critical amorphous thickness of more than 10 mm when they are cast in plates and more than 15 mm in rods.[9–14] Third, they have the lowest density (~2.0 g/cc), Young's modulus (~20 to 30 GPa), and shear modulus (~8 to 15 GPa) among all metallic glasses discovered so far.[24,25] Their Young's modulus values are comparable to the modulus of human bones, which makes the Ca-based metallic glasses attractive in biomedical research. Additional features of these alloys are low glass transition temperature ($T_g \sim 100$ °C to 190 °C), low crystallization temperature ($T_x \sim 130$ °C to 240 °C), and a wide temperature range of supercooled liquid ($\Delta T_x = T_x - T_g \sim 30$ °C to 80 °C).[9–14] Like many other glasses, the Ca-based BMGs are extremely brittle at room temperature and have good ductility in the supercooled liquid range.[11] While most Ca-based crystalline alloys oxidize in air in a matter of days, many Ca-based metallic glasses have improved oxidation resistance and retain shiny surfaces long after casting.[26] In the following sections, the composition and properties of Ca-based BMGs are described in more detail.

II. COMPOSITION, GFA, AND THERMAL PROPERTIES OF Ca-BASED BMGs

In this section, several Ca-based BMG systems are briefly overviewed, and their GFA, glass stability, and some characteristic properties, such as glass transition, crystallization, and melting temperatures, as well as heats of fusion and crystallization, are discussed relative to alloy compositions.

A. *Ternary Systems*

Figure 3 shows the Ca-rich corners of the liquidus projections of the Ca-Mg-Zn,[27] Ca-Mg-Cu,[28] and Ca-Mg-Al systems. While the liquidus projections for Ca-Mg-Zn and Ca-Mg-Cu were taken from the literature, the projection for the Ca-Mg-Al system has not been experimentally determined, and it was calculated using Pandat 5.0 software.[29] The composition ranges for BMGs predicted from Eq. [1] are bounded by dashed trapezoids, and the compositions of several produced alloys are marked as solid circles and their critical plate thicknesses also highlighted. Selected alloy compositions and their characteristic properties are tabulated in Table I. The presence of the ternary eutectic and peritectic reactions provides strong liquidus temperature gradients in the selected composition areas, which lead to high sensitivity of GFA with alloy composition (Figure 3). In an alloy group belonging to the same phase field in the liquidus projection, there is a tendency for GFA to increase with a decrease in the temperature difference between liquidus and solidus points, *i.e.*, with a decrease in the liquidus temperature, T_l (Table I).

For the Ca-Mg-Zn system, the alloys located in the $CaMg_2$ and Ca_3Zn phase fields have much better GFA than the alloys located in the Ca or $CaZn_2$ phase fields. For example, the alloys $Ca_{65}Mg_{20}Zn_{15}$ and $Ca_{60}Mg_{20}Zn_{20}$, which are located in the $CaMg_2$ phase field, have

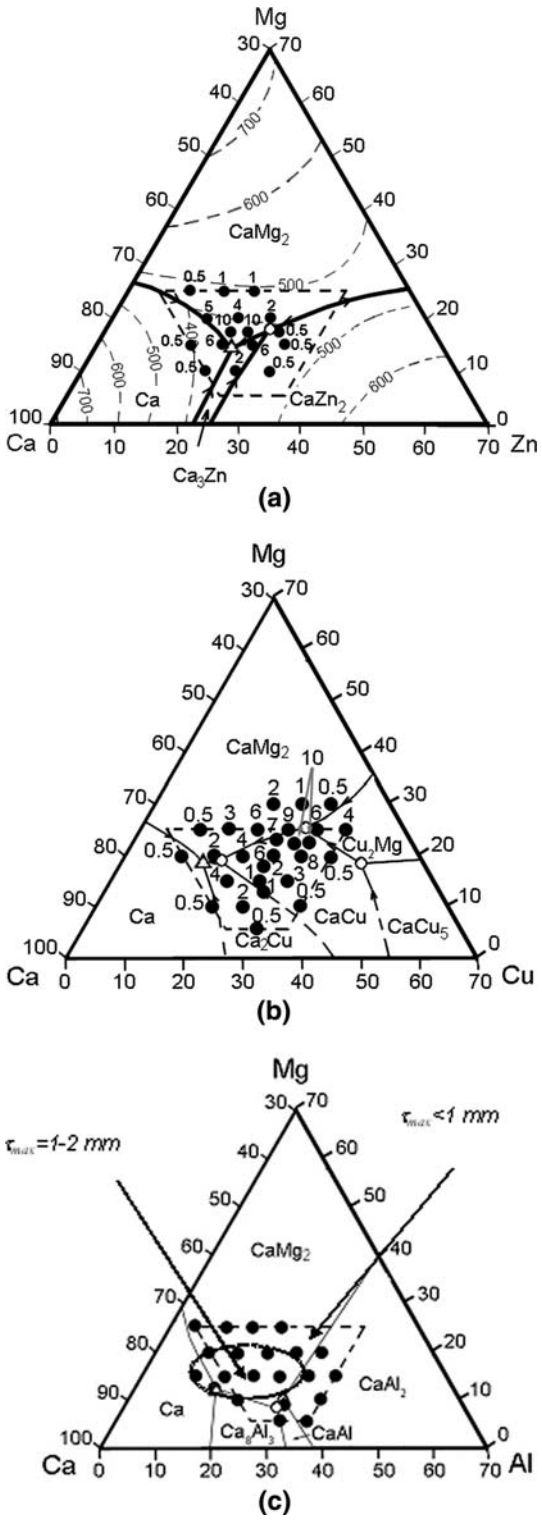

Fig. 3—Liquidus projections of (*a*) Ca-Mg-Zn, (*b*) Ca-Mg-Cu, and (*c*) Ca-Mg-Al systems. The projections show thick solid lines bounding the different phase fields. Ternary eutectic and peritectic reactions are marked by open triangles and open circles, respectively. A trapezoid with a dashed boundary on each projection represents a composition range for the ternary BMGs, according to Eq. [1]. The compositions of several amorphous alloys are shown as solid circles. The maximum fully amorphous plate thicknesses (τ_{max}, in millimeters) achieved for these alloys are shown as pertinent numbers in (a) and (b) and highlighted for two selected regions in (c).

τ_m = 5 and 4 mm, respectively, while the alloys with the same temperature interval for solidification (the same liquidus temperature) but with compositions corresponding to the Ca or $CaZn_2$ phase field have $\tau_m < 0.5$ mm. These results suggest that the driving force for crystallization of the $CaMg_2$ phase should be much lower than those of Ca and $CaZn_2$ phases. The alloys $Ca_{62.5}Mg_{17.5}Zn_{20}$ and $Ca_{60}Mg_{17.5}Zn_{22.5}$, which are located in the $CaMg_2$ phase field near the eutectic point, have the best GFA (τ_m = 10 mm), while all alloys located in the $CaZn_2$ phase field have the poorest GFA (τ_m = 0.5 mm).

Ca-Mg-Zn metallic glasses have very low glass transition, T_g, crystallization, T_x, and melting, T_m, temperatures.[9] For example, depending on the alloy composition, T_g is in the range of 92 °C to 116 °C and T_x is from 124 °C to 155 °C, providing a supercooled liquid temperature range, $\Delta T_x = T_x - T_g$, from 30 °C to 50 °C. All produced alloys showed eutectic melting at $T_m \approx 336$ °C, and the heat of fusion varied from 142 to 213 J/g.[9] The best glass formers in this system, which showed a critical plate thickness $\tau_{max} \geq 10$ mm, are $Ca_{60}Mg_{17.5}Zn_{22.5}$ (T_g = 110 °C, ΔT_x = 38 °C, and $T_{rg} = T_g/T_l = 0.59$) and $Ca_{62.5}Mg_{17.5}Zn_{20}$ (T_g = 102 °C, ΔT_x = 37 °C, and T_{rg} = 0.59) (Table I).

In contrast to the Ca-Mg-Zn system, no apparent correlation between the reported eutectic composition[28] and GFA was initially found for the Ca-Mg-Cu system (Figure 3(b)). However, detailed analysis of the solidus and liquidus temperatures for the alloys conducted in Reference 12 revealed that the location of the eutectic reaction on the Ca-Mg-Cu phase diagram, reported by Myles[28] and shown in Figure 3(b), is incorrect and that the eutectic reaction should be present at around 50 to 53 at. pct Ca and 23 to 25 at. pct Mg, with a melting temperature of ~354 °C. The fact that two alloys, $Ca_{50}Mg_{25}Cu_{25}$ and $Ca_{53}Mg_{23}Cu_{24}$, which are located near the identified eutectic point, have the lowest melting temperature ($T_m \approx 354$ °C) and the lowest melting range, $\Delta T_m = T_l - T_m$, of ~28 °C, confirms this finding. At the same time, a peritectic reaction at $T_m \approx 386$ °C and at higher Ca concentrations (around 70 pct Ca and ~15 pct Mg) was suggested[11,12] instead of the eutectic reaction shown in Figure 3(b). In view of these corrections to the liquidus projection, it appears that the best Ca-Mg-Cu glass forming alloys (with the maximum plate thickness in the range of 6 to 10 mm) have near-eutectic compositions, while the poorest glass forming alloys are located far from the identified eutectic and have a large freezing range or high melting temperatures due to the occurrence of peritectic reactions. Such behavior is now in agreement with previous experimental observations, indicating the importance of eutectic reactions for glass formation,[1] and it is also consistent with the behavior in the Ca-Mg-Zn system, which was discussed previously.

The Ca-Mg-Cu metallic glasses have slightly higher T_g, T_x, and T_m[11,12] than the Ca-Mg-Zn glasses. For example, T_g is in the range from 110 °C to 133 °C and T_x is from 132 °C to 169 °C, providing the supercooled liquid temperature range, $\Delta T_x = T_x - T_g$, from 19 °C to

Table I. Composition, Maximum Thickness (τ_m), Glass Transition (T_g), Crystallization (T_x), Solidus (T_m), and Liquidus (T_l) Temperatures, and Heats of Crystallization (ΔH_x) and Fusion (ΔH_m) for Selected Ca-Mg-Zn, Ca-Mg-Cu, and Ca-Mg-Al Ternary Glassy Alloys

Alloy Composition	τ_m (mm)	T_g (°C)	T_x (°C)	T_m (°C)	T_l (°C)	ΔH_x (J/g)	ΔH_m (J/g)
Ca-Mg-Zn[8,9]							
$Ca_{55}Mg_{20}Zn_{25}$	2.0	110	155	350	429	82	170
$Ca_{60}Mg_{15}Zn_{25}$	6.0	106	154	336	377	99	154
$Ca_{60}Mg_{17.5}Zn_{22.5}$	10.0	105	155	336	377	115	167
$Ca_{60}Mg_{20}Zn_{20}$	4.0	105	142	336	387	90	153
$Ca_{62.5}Mg_{17.5}Zn_{20}$	10.0	102	139	336	367	109	150
$Ca_{65}Mg_{15}Zn_{20}$	6.0	102	137	336	357	109	147
Ca-Mg-Cu[11,12]							
$Ca_{40}Mg_{25}Cu_{35}$	4.0	126	163	377	407	89	196
$Ca_{45}Mg_{25}Cu_{30}$	6.0	127	165	354	405	132	222
$Ca_{47.5}Mg_{22.5}Cu_{30}$	10.0	126	167	352	400	154	219
$Ca_{50}Mg_{25}Cu_{25}$	9.0	127	166	354	382	129	210
$Ca_{50}Mg_{22.5}Cu_{27.5}$	10.0	127	169	354	390	150	208
$Ca_{50}Mg_{20}Cu_{30}$	8.0	128	169	355	417	139	378
$Ca_{53}Mg_{23}Cu_{24}$	7.0	133	166	354	382	134	196
$Ca_{55}Mg_{25}Cu_{20}$	8.0	125	155	354	395	125	226
$Ca_{58}Mg_{18}Cu_{24}$	6.0	115	153	355	394	119	186
$Ca_{60}Mg_{20}Cu_{20}$	4.0	114	139	356	405	105	181
$Ca_{65}Mg_{15}Cu_{20}$	4.0	110	136	357	409	115	195
Ca-Mg-Al[15,30]							
$Ca_{58}Mg_{10}Al_{32}$	1.5	240	266	472	> 600	104	> 275
$Ca_{60}Mg_{10}Al_{30}$	2.0	235	250	475	600	124	309
$Ca_{65}Mg_{15}Al_{20}$	1.5	190	218	413	503	175	271
$Ca_{70}Mg_{15}Al_{15}$	1.5	147	187	414	498	146	213

43 °C. Several characteristic melting points were identified as a eutectic reaction (~354 °C) and three peritectic reactions (~363 °C, ~375 °C, and ~397 °C), and the heat of fusion varied from 155 to 378 J/g.[12] The best glass formers in this system, which showed a critical plate thickness $\tau_{max} \geq 10$ mm are $Ca_{50}Mg_{22.5}Cu_{27.5}$ (T_g = 127 °C, ΔT_x = 42 °C, and T_{rg} = 0.60) and $Ca_{47.5}Mg_{22.5}Cu_{30}$ (T_g = 126 °C, ΔT_x = 41 °C, and T_{rg} = 0.59) (Table I).

The GFA of Ca-Mg-Al metallic glasses was not as good as that of Ca-Mg-Zn or Ca-Mg-Cu (Figure 3). The maximum amorphous thicknesses achieved for the Ca-Mg-Al alloys, both in plates and rods, were in the range of ~1 to 2 mm,[15,30] and the bulk glassy alloys were produced in a much narrower composition range (identified by an oval area in Figure 3(c)). This composition range corresponds to the $CaMg_2$ phase field and is close to the eutectic composition. Although the Ca-Mg-Al alloys have a reduced GFA, they have an increased stability against crystallization, which is manifested in an increase in both T_g and T_x. Indeed, depending on the alloy composition, T_g varies from 130 °C to 240 °C, T_x from 152 °C to 282 °C, and ΔT_x from 20 °C to 57 °C.[15,30] The best glass formers in this system, which show a critical plate thickness $\tau_{max} \sim 2$ mm, are $Ca_{70}Mg_{15}Al_{15}$ (T_g = 147 °C, ΔT_x = 40 °C, and T_{rg} = 0.54) and $Ca_{65}Mg_{15}Al_{20}$ (T_g = 190 °C, ΔT_x = 28 °C, and T_{rg} = 0.60) (Table I). The Ca-Mg-Al glasses do not contain heavy transition metals, and, therefore, they have the lowest densities among all Ca-based metallic glasses, as well as all other glasses. Their density varies in the range from 1.62 g/cm^3 ($Ca_{80}Mg_{15}Al_5$) to 1.79 g/cm^3 ($Ca_{50}Mg_{15}Al_{35}$).

B. *Quaternary and Quinternary Systems*

Glass forming abilities in three Ca-based quaternary systems have been extensively studied recently. These are Ca-Mg-Zn-Cu,[11] Ca-Mg-Al-Zn,[30] and Ca-Mg-Al-Cu,[30] and their composition and thermal properties are listed in Table II. The Ca-Mg-Zn-Cu alloys were produced by partial replacement of Cu with Zn in Ca-Mg-Cu alloys or by replacing Zn with Cu in Ca-Mg-Zn alloys. Combined additions of Zn and Cu generally improve GFA. For example, the ternary $Ca_{55}Mg_{18}Zn_{27}$ alloy has τ_m = 0.5 mm, T_g = 116 °C, $\Delta T_x = T_x - T_g$ = 30 °C, and $T_{rg} = T_g/T_l$ = 0.58. Partial replacement of Zn by Cu leads to a very good glass forming alloy $Ca_{55}Mg_{18}Zn_{11}Cu_{16}$ that has $\tau_m >$ 10 mm, T_g = 103 °C, ΔT_x = 53 °C, and T_{rg} = 0.60. Another example is modification of a ternary $Ca_{58}Mg_{18}Cu_{24}$ glassy alloy, which has τ_m = 6 mm, T_g = 115 °C, ΔT_x = 38 °C, and T_{rg} = 0.58. After replacing half the Cu with Zn, the GFA increases significantly and the resulting alloy $Ca_{58}Mg_{18}Zn_{12}Cu_{12}$ has $\tau_m >$ 10 mm, T_g = 100 °C, ΔT_x = 55 °C, and T_{rg} = 0.60. On the other hand, substitution of Mg by Zn or Cu reduces GFA if the amount of Mg decreases below 15 at. pct. The Ca-Mg-Zn-Cu glasses have T_g values in the range from 100 °C to 128 °C, T_x from 154 °C to 168 °C, and ΔT_x from 32 °C to 66 °C. The melting temperature is in the range of 325 °C to 354 °C, and the temperature interval of melting is 21 °C to 120 °C (Table II). Similar to the ternary alloy systems, there is a tendency for the GFA of these quaternary alloys to improve with a decrease in the melting range ($\Delta T_l = T_l - T_m$), indicating that the best glass formers have near-eutectic compositions.

Table II. Composition, Maximum Thickness (τ_m), Glass Transition (T_g), Crystallization (T_x), Solidus (T_m), and Liquidus (T_l) Temperatures, and Heats of Crystallization (ΔH_x) and Fusion (ΔH_m) for Ca-Mg-Zn-Cu, Ca-Mg-Al-Zn, Ca-Mg-Al-Cu, and Ca-Mg-Al-Zn-Cu Glassy Alloys

Alloy Composition	τ_m (mm)	T_g (°C)	T_x (°C)	T_m (°C)	T_l °C	ΔH_x (J/g)	ΔH_m (J/g)
Ca-Mg-Zn-Cu							
$Ca_{42.5}Mg_{21.5}Zn_{15}Cu_{21.5}$	4.0	128	162	354	385	108	179
$Ca_{45}Mg_{22.5}Zn_{10}Cu_{22.5}$	6.0	127	162	354	382	110	176
$Ca_{47}Mg_{19}Zn_7Cu_{27}$	6.0	120	167	334	403	122	198
$Ca_{47.5}Mg_{23.75}Zn_5Cu_{23.75}$	8.0	126	163	335	384	125	197
$Ca_{50}Mg_{10}Zn_{15}Cu_{25}$	2.0	122	154	325	429	112	169
$Ca_{50}Mg_{15}Zn_{10}Cu_{25}$	10.0	122	161	327	405	113	187
$Ca_{50}Mg_{20}Zn_5Cu_{25}$	10.0	126	168	338	381	139	194
$Ca_{50}Mg_{25}Zn_5Cu_{20}$	8.0	120	162	336	390	102	198
$Ca_{50}Mg_{25}Zn_{10}Cu_{15}$	10.0	121	164	325	434	99	219
$Ca_{50}Mg_{25}Zn_{15}Cu_{10}$	8.0	110	157	330	450	97	202
$Ca_{55}Mg_{11}Zn_{11}Cu_{23}$	1.0	106	157	328	444	97	167
$Ca_{55}Mg_{18}Zn_{11}Cu_{16}$	> 10.0	100	166	330	363	119	166
$Ca_{55}Mg_{18}Zn_{16}Cu_{11}$	> 10.0	111	164	331	352	117	170
$Ca_{58}Mg_{18}Zn_{12}Cu_{12}$	> 10.0	100	155	328	355	102	138
Ca-Mg-Al-Zn[30]							
$Ca_{48}Mg_{13}Al_{19}Zn_{20}$	0.5	163	214	375	540	70	114
$Ca_{55}Mg_{18}Al_{20}Zn_7$	1.0	174	218	352	549	76	189
$Ca_{55}Mg_{20}Al_{10}Zn_{15}$	3.5	130	196	358	500	76	179
$Ca_{55}Mg_{20}Al_{15}Zn_{10}$	2.0	148	204	334	533	91	262
$Ca_{55}Mg_{20}Al_{19}Zn_6$	1.5	175	211	358	472	92	223
$Ca_{60}Mg_{15}Al_{10}Zn_{15}$	4.0	130	201	350	430	99	124
$Ca_{60}Mg_{18}Al_{15}Zn_7$	2.5	158	212	348	475	110	203
$Ca_{60}Mg_{20}Al_{10}Zn_{10}$	6.0	130	176	334	473	95	181
Ca-Mg-Al-Cu[30]							
$Ca_{50}Mg_{20}Al_{10}Cu_{20}$	1.0	138	168	384	458	96	227
$Ca_{50}Mg_{22.5}Al_5Cu_{22.5}$	3.5	143	183	354	489	100	188
$Ca_{60}Mg_9Al_{11}Cu_{20}$	2.0	128	177	383	484	117	185
$Ca_{60}Mg_{15}Al_{10}Cu_{15}$	2.0	124	157	384	537	103	165
$Ca_{60}Mg_{20}Al_{10}Cu_{10}$	2.0	135	169	390	544	96	210
Ca-Mg-Al-Zn-Cu[30]							
$Ca_{55}Mg_{18}Al_5Zn_{11}Cu_{11}$	9	119	175	331	513	114	192
$Ca_{55}Mg_{18}Al_{10}Zn_{11}Cu_6$	3	128	171	341	562	101	228
$Ca_{55}Mg_{18}Al_{15}Zn_6Cu_6$	2.5	136	177	360	581	95	293
$Ca_{60}Mg_{18}Al_{10}Zn_6Cu_6$	5	134	176	357	530	128	211
$Ca_{60}Mg_{18}Al_{15}Zn_3Cu_4$	2	144	195	370	503	123	193

Quaternary Ca-Mg-Al-Zn and Ca-Mg-Al-Cu glasses were produced from baseline ternary Ca-Mg-Zn and Ca-Mg-Cu alloys, respectively, by a partial substitution of Zn or Cu with Al.[31] Addition of Al was found to reduce GFA; however, this considerably improved the glass stability. Indeed, both the glass transition and crystallization temperatures increased significantly. For example, T_g values are in the range of 124 °C to 175 °C, T_x from 157 °C to 218 °C, and ΔT_x from 30 °C to 71 °C. Fully amorphous plates with maximum thicknesses of 6 and 3.5 mm were produced from $Ca_{60}Mg_{20}Al_{10}Zn_{10}$ and $Ca_{50}Mg_{22.5}Al_5Cu_{22.5}$, respectively.

Table II also lists thermal properties of several quinternary Ca-Mg-Al-Zn-Cu glasses. Their glass transition temperatures vary from 105 °C to 150 °C and ΔT_x from 40 °C to 60 °C. The reduced glass transition temperatures are in the range of 0.46 to 0.56. For example, a $Ca_{55}Mg_{18}Al_5Zn_{11}Cu_{11}$ glassy alloy, which has $\tau_{max} = 9$ mm, has $T_g = 119$ °C, $\Delta T_x = 56$ °C, and $T_{rg} = 0.50$.

C. *Correlation between the GFA and Onset Driving Force for Crystallization in Ca-Based Glasses*

Liquid can be undercooled and form the glassy state only if crystallization is kinetically or thermodynamically constrained. A thermodynamic analysis of the onset driving force (ODF) for crystallization of supercooled liquids was recently conducted to explain the strong composition dependence of GFA in the Ca-Mg-Zn ternary alloy system observed experimentally.[32] The ODFs for primary crystallization of various possible phases from the undercooled liquid to a temperature, which is close to T_g for the Ca-Mg-Zn alloys, were calculated as a function of the Ca and Mg contents using critically assessed thermodynamic parameters,[33] based on the CALPHAD method.[34] Although the liquid phase was described as a disordered liquid solution and short-range ordering was not taken into account, the model showed good agreement with the experiment. The results showed that the best glass forming Ca-Mg-Zn compositions correspond to local minima of the ODFs.

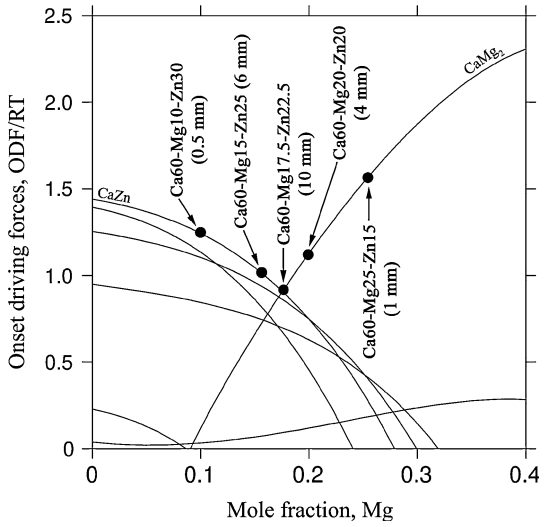

Fig. 4—Calculated onset driving forces of various crystalline phases for $Ca_{60}Mg_xZn_{100-x}$ alloys *vs* Mg content at 390 K (117 °C).[32] Filled circles represent the alloy compositions studied. Their critical thicknesses are indicated.

As an example, Figure 4 shows the calculated ODFs in the $Ca_{60}Mg_XZn_{100-X}$ system. The calculations predict that the undercooled liquid starts to crystallize by formation of two phases: CaZn at a lower Mg content (< 17.5 pct) and $CaMg_2$ at a larger amount of Mg. The local minimum of the ODF is located at ~17.5 pct Mg, predicting the best GFA for the alloy $Ca_{60}Mg_{17.5}Zn_{22.5}$ in this alloy series, in agreement with experimental results. Indeed, this alloy has a maximum critical thickness of 10 mm, and the critical thickness for the $Ca_{60}Mg_XZn_{100-X}$ alloys decreases with an increase in the ODF.[9,32] Similar correlations between ODF and GFA have recently been obtained for other glass forming systems, such as Cu-Ti-Zr[35] and Cu-Mg-Y[36] ternary systems, which may indicate universality of this method for predicting alloys with good GFA.

III. LIQUID FRAGILITY OF Ca-BASED BMGS

The dynamic viscosity, η, and the Maxwell relaxation time, τ, of supercooled liquids are important parameters to describe the time scale for structural rearrangement of atoms in a liquid required for the growth of crystal nuclei. These two parameters are related through the "infinite frequency" shear modulus, G_∞:[37] $\eta = G_\infty\tau$, and typical G_∞ values are of the order of 10^{10} Pa.[38] The exceptional stability of BMG alloys against crystallization during solidification should therefore be related to their high viscosity/relaxation time in the temperature range between T_l and T_g. The temperature dependence of the relaxation time is generally described by the Vogel–Fulcher–Tammann (VFT) equation:[39]

$$\tau = \tau_o \exp\left(\frac{DT_o}{T - T_o}\right) \qquad [2]$$

where $\tau_o \approx 10^{-14}$ s is the relaxation time at an infinitely high temperature; T_o is the VFT temperature at which τ becomes infinite; and D is the strength parameter that characterizes liquid fragility, *i.e.*, the level of departure from Arrhenius behavior. When D is high (≥70 to 100), the behavior is essentially Arrhenius, *i.e.*, log τ increases almost linearly with an increase in T_g/T, and the liquid is called a strong liquid. With a decrease in D (especially below ~10 to 20), the behavior becomes strongly non-Arrhenius, *i.e.*, the liquid exhibits a weak dependence of log τ on T_g/T at $T \approx T_l$ and a very strong dependence at $T \approx T_g$, and such liquid is called fragile liquid. Very good glass forming oxides, such as SiO_2 and GeO_2, are examples of strong liquids, and very poor glass forming metals or organics, such as O-terphenil, are examples of very fragile liquids.[39,40]

The relaxation behavior of three Ca-based BMGs, $Ca_{65}Mg_{15}Zn_{20}$, $Ca_{50}Mg_{20}Cu_{30}$, and $Ca_{55}Mg_{18}Zn_{11}Cu_{16}$, in the supercooled liquid range, near the glass transition temperature, was studied using a DSC method, which is well described in Reference 41, and the experimental results are presented in Figure 5 in the form of an Angell plot.[39] These experimental points were fitted with the VFT Eq. [2], and the fitting parameters are given in Table III. The known data for two other BMGs (Zr-based glass Vit4[42] and Mg-based $Mg_{65}Cu_{25}Y_{10}$[43]) and a strong oxide glass (SiO_2) are also plotted in Figure 5 for comparison. It can be seen from Figure 5 that the liquid behavior of $Ca_{65}Mg_{15}Zn_{20}$ is the strongest,

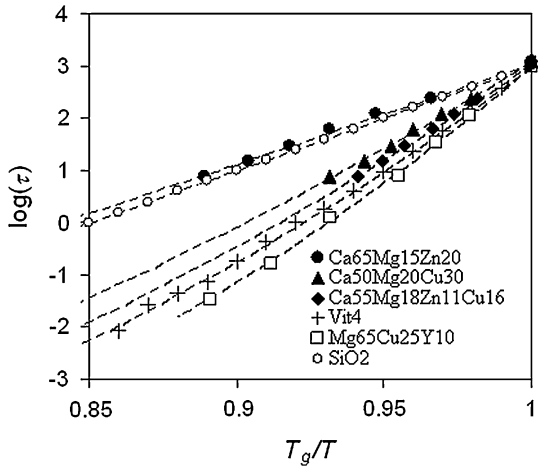

Fig. 5—Dependence of the relaxation time, τ, on the reciprocal temperature, T, scaled by T_g for (●) $Ca_{65}Mg_{15}Zn_{20}$, (▲) $Ca_{50}Mg_{20}Cu_{30}$, and (♦) $Ca_{55}Mg_{18}Zn_{11}Cu_{16}$ (current work); (+) $Zr_{46.75}Ti_{8.25}Cu_{7.5}Ni_{10}Be_{27.5}$ (Vit4),[42] (□) $Mg_{65}Cu_{25}Y_{10}$,[43] and (○) SiO_2[40] glass forming liquids. Dashed lines are fits of Eq. [3].

Table III. Fitting Parameters of the Vogel–Fulcher–Tammann Equation [3] and the Temperature T_3 Corresponding to τ = 1000 Seconds for Three Ca-Based Metallic Glasses, Zr-Based Glass, and Mg-Based Glass

Composition (At. Pct)	τ_o (s)	D	T_o (K)	T_3 (K)
$Ca_{65}Mg_{15}Zn_{20}$	1.0×10^{14}	287	41	341
$Ca_{50}Mg_{20}Cu_{30}$	1.0×10^{14}	38	194.3	382
$Ca_{55}Mg_{18}Zn_{11}Cu_{16}$	1.0×10^{14}	30	212.5	375
$Zr_{46.75}Ti_{8.25}Cu_{7.5}Ni_{10}Be_{27.5}$ (Vit4)[42]	2.5×10^{13}	22.7	372	596
$Mg_{65}Cu_{25}Y_{10}$[43]	2.1×10^{14}	22.1	260	404

and the relaxation time for this alloy at the same T_g/T values is even higher than that for SiO_2. Two other Ca-based alloys, which contain Cu, are more fragile than $Ca_{65}Mg_{15}Zn_{20}$; however, they are stronger than the Zr- and Mg-based BMGs. One can therefore suggest that the strong liquid behavior of the Ca-based BMGs is one of the reasons for their excellent GFA.

IV. DENSITY OF Ca-BASED BMGS

If the densities of pure elements are known, the theoretical density of an alloy containing these elements can be calculated using the following formula:

$$\rho = \frac{\sum_{i=1}^{n} M_i X_i}{\sum_{i=1}^{n} \frac{M_i X_i}{\rho_i}} \quad [3]$$

where ρ_i and M_i are the density and atomic weight of a pure element i, and X_i is the atomic fraction of this element in the alloy consisting of n elements. This theoretical density can then be compared with the experimentally measured density in order to estimate the packing efficiency or the presence of voids or other defects. The results for three Ca-based glasses are presented in Table IV. The densities of these alloys were determined by precise measurements of the volume and weight of several samples. The density of $Ca_{65}Mg_{15}Zn_{20}$ was found to be about 0.63 pct lower than the theoretical density; however, the measured density of two other metallic glasses, which contain Cu, were considerably higher than the theoretical density, and this difference is much higher than can be explained by experimental error. This result is rather unusual because the density of a glassy state is generally smaller than the density of its crystalline counterpart, for which the theoretical density is a good approximation. This discrepancy can be explained if very dense packing of elements in these metal glasses is suggested. Indeed, the theoretical density of an alloy is calculated from the densities of pure metals under the assumption that the volume per element in the produced alloy is the same as it is in the pure metal and that the elements occupy similar atomic sites, which can be incorrect, especially when the elements occupy interstitial sites in the alloy. The atomic size of Cu is ~35 pct smaller than the size of Ca. Therefore, Cu can fill voids between large Ca atoms in the amorphous structure, producing Cu-centered clusters and leading to a density above the theoretical density, which is however restricted in the crystalline state by long-range ordering. Recent studies[12] have shown that Ca-based metallic glasses containing Cu have shorter interatomic distances resulting from a mixture of metallic and covalent bonding. This can also lead to denser packing and a higher density of the Ca-based metallic glasses.

Table IV. Theoretical, ρ_T, and Experimentally Measured, ρ_E, Densities of Ca-Based BMGs

Alloy	ρ_T, g/cm^3	ρ_E, g/cm^3	$100(\rho_E - \rho_T)/\rho_T$, Pct
$Ca_{65}Mg_{15}Zn_{20}$	2.063	2.050 ± 0.020	–0.63 ± 0.96
$Ca_{55}Mg_{18}Zn_{11}Cu_{16}$	2.319	2.411 ± 0.018	3.97 ± 0.83
$Ca_{50}Mg_{20}Cu_{30}$	2.463	2.589 ± 0.025	5.12 ± 1.0

V. ELASTIC PROPERTIES

The elastic properties of three Ca-based BMGs, $Ca_{65}Mg_{15}Zn_{20}$, $Ca_{50}Mg_{20}Cu_{30}$, and $Ca_{55}Mg_{18}Zn_{11}Cu_{16}$, were studied by Zhang *et al.*[25] using resonant ultrasound spectroscopy. Longitudinal and shear moduli were experimentally measured in the temperature range from 0 to 400 K, and then other elastic constants, such as Young's modulus, bulk modulus, Lame's constant, and Poisson's ratio, were calculated under the assumption that the glasses are isotropic. The temperature dependences of the shear, bulk, and Young's moduli and the Poisson's ratio are shown in Figure 6, and the values of these parameters at room temperature are given in Table V. A clear transition in the temperature dependence of the elastic constants is observed at ~362 K for $Ca_{65}Mg_{15}Zn_{20}$, ~386 K for $Ca_{55}Mg_{18}Zn_{11}Cu_{16}$, and ~400 K for $Ca_{50}Mg_{20}Cu_{30}$. Below the transition temperature, all moduli decrease, while the Poisson ratio increases, with increasing temperature. Above the transition temperature, the rate of softening significantly decreases or is fully arrested. This transition was found to be due to the start of crystallization in the heated specimens. The elastic moduli of these Ca-based BMGs are rather low, and they increase with an increase in the amount of Cu and a decrease in the amount of Ca.

VI. HEAT CAPACITY AND LOCALIZED EINSTEIN MODES IN Ca-BASED BMGS

The temperature dependence of the heat capacity C_p of several Ca-based metallic glasses was reported recently.[24] Analysis of these results led to a conclusion that the specific heat in these glasses cannot be described with the Debye model alone and a localized Einstein mode should be taken into account. Figure 7 shows the specific heat *vs* temperature for $Ca_{50}Mg_{20}Cu_{30}$, $Ca_{55}Mg_{18}Zn_{11}Cu_{16}$, and $Ca_{65}Mg_{15}Zn_{20}$ BMGs, together with a model calculation including the contributions of the Debye model and a single Einstein mode. The solid line through the data represents a fit to the equation

$$C_p = \gamma T + n_D C_D + n_E C_E \quad [4]$$

where γT describes the electron contribution (which can be determined at the lowest temperatures), C_D is the Debye integral $9R\left(\frac{T}{\theta_D}\right)^3 \int_0^{\theta_D} \frac{x^4 e^x}{(e^x-1)^2} dx$ (with θ_D the Debye temperature), and C_E is the contribution of an Einstein mode given by $C_E = 3R\left(\frac{\theta_E}{T}\right)^2 \frac{e^{\theta_E/T}}{(e^{\theta_E/T}-1)^2}$ (with θ_E the Einstein temperature). The terms n_D and n_E represent

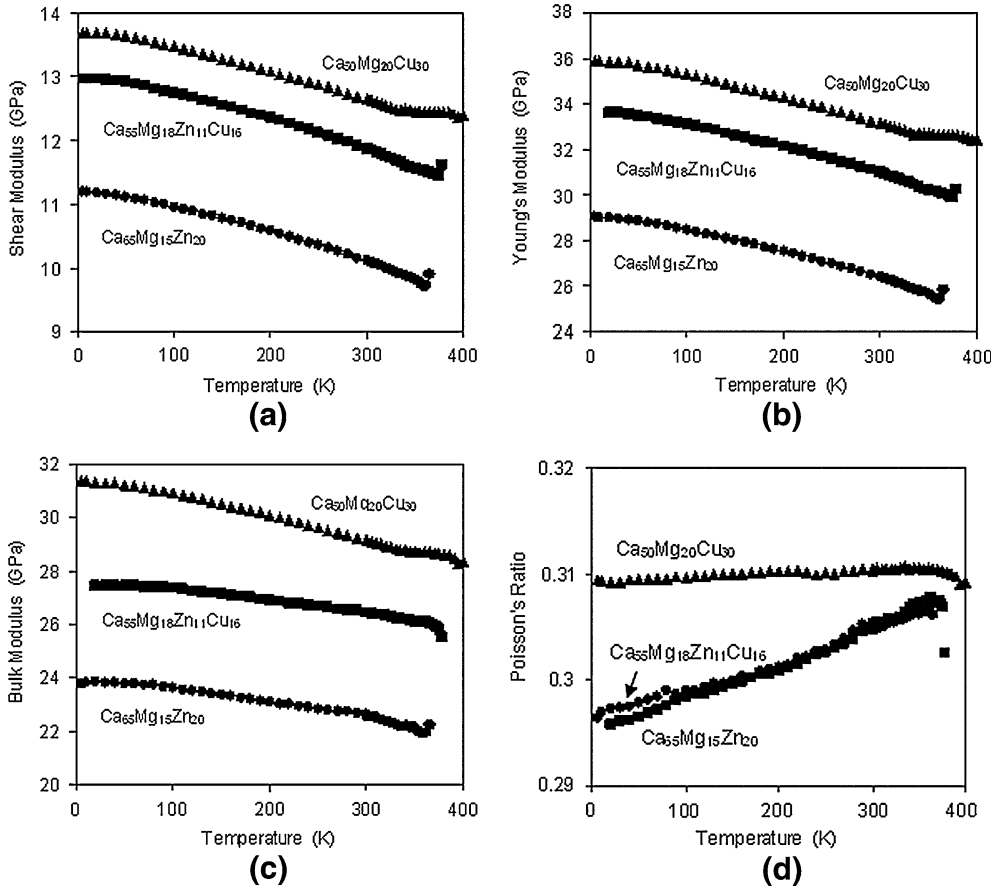

Fig. 6—The temperature dependences of (*a*) shear, (*b*) Young's, and (*c*) bulk moduli and (*d*) Poisson's ratio.[25]

Table V. Elastic Parameters of Ca-Based BMGs at Different Temperatures

Alloy	$Ca_{65}Mg_{15}Zn_{20}$				$Ca_{55}Mg_{18}Zn_{11}Cu_{16}$				$Ca_{50}Mg_{20}Cu_{30}$			
T (K)	*G* (GPa)	*E* (GPa)	*B* (GPa)	ν	*G* (GPa)	*E* (GPa)	*B* (GPa)	ν	*G* (GPa)	*E* (GPa)	*B* (GPa)	ν
50	11.1	28.9	23.8	0.298	12.9	33.5	27.4	0.297	13.6	35.7	31.3	0.310
100	11.0	28.5	23.6	0.299	12.8	33.1	27.4	0.298	13.5	35.3	30.9	0.310
150	10.8	28.0	23.4	0.300	12.6	32.6	27.1	0.300	13.3	34.8	30.5	0.310
200	10.6	27.5	23.1	0.301	12.4	32.2	26.9	0.301	13.1	34.3	30.1	0.310
250	10.4	27.0	22.8	0.303	12.1	31.6	26.7	0.303	12.9	33.8	29.6	0.310
300	10.1	26.4	22.6	0.305	11.9	31.0	26.5	0.305	12.7	33.2	29.2	0.311
350	9.8	25.7	22.1	0.306	11.6	30.2	26.1	0.307	12.5	32.7	28.7	0.311

the fraction of, respectively, Debye and Einstein modes per mole of atoms. An excellent agreement for all three alloys is reached for a Debye temperature $\theta_D = 255$ K and an Einstein temperature $\theta_E = 80$ K. Only the Einstein oscillator strength is different for the three Ca-based BMGs, with $n_E = 0.10$ for $Ca_{50}Mg_{20}Cu_{30}$, $n_E = 0.12$ for $Ca_{55}Mg_{18}Zn_{11}Cu_{16}$, and $n_E = 0.16$ for $Ca_{65}Mg_{15}Zn_{20}$. A decrease in the Einstein oscillator strength with an increase in the amount of Cu has been explained by an increasing covalent character[24] to the dominant metallic bonding in these metallic glasses. A similar temperature behavior of the heat capacity was also observed in binary $Cu_{50}Zr_{50}$ glasses, as well as more complex amorphous metallic alloys such as $Zr_{46.5}Ti_{8.25}Cu_{7.5}Ni_{10}Be_{27.5}$.[44,45]

In the past few years, a number of metallic solids have been identified where thermodynamic properties were shown to be dominated by the presence of Einstein oscillators.[46–48] In these cases, the Einstein modes were related to weakly bound "rattling" atoms, which reside in the oversized cages that characterize the structure of these solids. In the case of BMGs, the origin of the local modes remains unclear: the presence of weakly bound atoms is not obvious, even though it has been suggested that the vibrations of solute atoms in the compound could induce independent localized modes.[44] Another issue concerns the excess density of states—the so-called boson-peak—found in glasses. It is tempting to link the Einstein modes to the boson peak, even though at this time there is no evidence that both are related. A careful

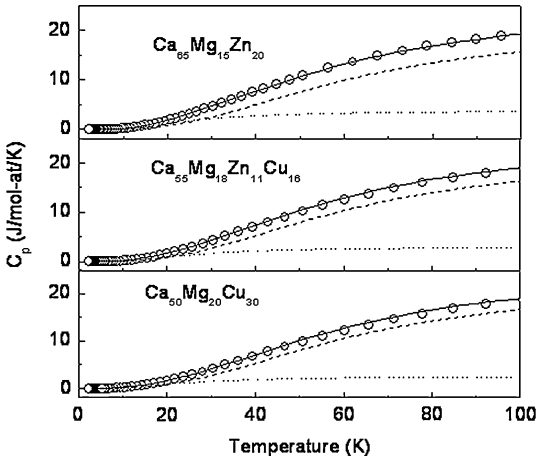

Fig. 7—Specific heat C_p *vs* temperature for $Ca_{50}Mg_{20}Cu_{30}$, $Ca_{55}Mg_{18}Zn_{11}Cu_{16}$, and $Ca_{65}Mg_{15}Zn_{20}$. ○: experimental data, dotted line: contribution of Einstein oscillator with $\Delta = 80$ K, dashed line: Debye C_p ($\theta_D = 255$ K) + γT, and solid line: model calculation including both Einstein and Debye contributions.[24]

study of the boson peak in the Ca-based glasses will need to be carried out in order to elucidate this issue.

VII. COMPRESSION PROPERTIES

The Ca-based BMGs are very brittle at room temperature; however, in the temperature range of the supercooled liquid, *i.e.*, at $T_g \le T < T_x$, they can be plastically deformed by compression without fracture up to ~20 pct.[11] The compression stress-strain curves for a $Ca_{47}Mg_{19}Zn_7Cu_{27}$ glassy alloy deformed at different temperatures are shown in Figure 8. At room temperature, an as-cast amorphous sample was loaded to ~2 pct elastic strain and then exploded into powder. During compression at 110 °C, 120 °C, and 130 °C, yielding occurred and the flow stress decreased during plastic deformation (Figure 8(b)). After preliminary 10 pct plastic strain at 120 °C, this amorphous alloy showed some (~0.3 pct) plastic strain at room temperature before brittle fracture (Figure 8(a)).

The extremely brittle behavior of Ca-based BMGs at room temperature can be due to their low Poisson's ratio,[25] an increasing proportion of covalent bonding,[12] and their very low fragility. Indeed, it has long been known for crystalline metals,[49] and has recently been shown for metallic glasses,[50] that the brittleness correlates with the Poisson's ratio ν, so that when ν decreases below a critical value, the metal becomes brittle. For many metallic glasses, this critical value is $\nu_{cr} \approx 0.32$,[50–52] while the Poisson's ratios of Ca-based glasses at room temperature are much below 0.32 (Table V). The covalent bonding and strong liquid behavior are known to suppress atom mobility, also leading to brittleness.

An increase in the ductility above the glass transition temperature is common for amorphous metallic alloys, and it is explained by transformation of the glassy state into a super-cooled liquid state, which is accompanied by a decrease in viscosity.[53,54] The strain-induced softening is generally explained by an increase in the free volume and generation of shear bands with dislocation-like defects.[53–56] Development of some room-temperature ductility after preliminary high-temperature deformation is a rather interesting observation. Very brittle behavior at room temperature is due to random atomic arrangement and difficulty to initiate shear in the as-cast amorphous alloy. High elastic energy accumulated during sample loading results in stress concentrations in chemically weak regions, leading to explosion-like fracture. On the other hand, preliminary plastic deformation at a higher temperature creates a number of shear bands in an amorphous sample,[55] which can be activated during following room-temperature compression.

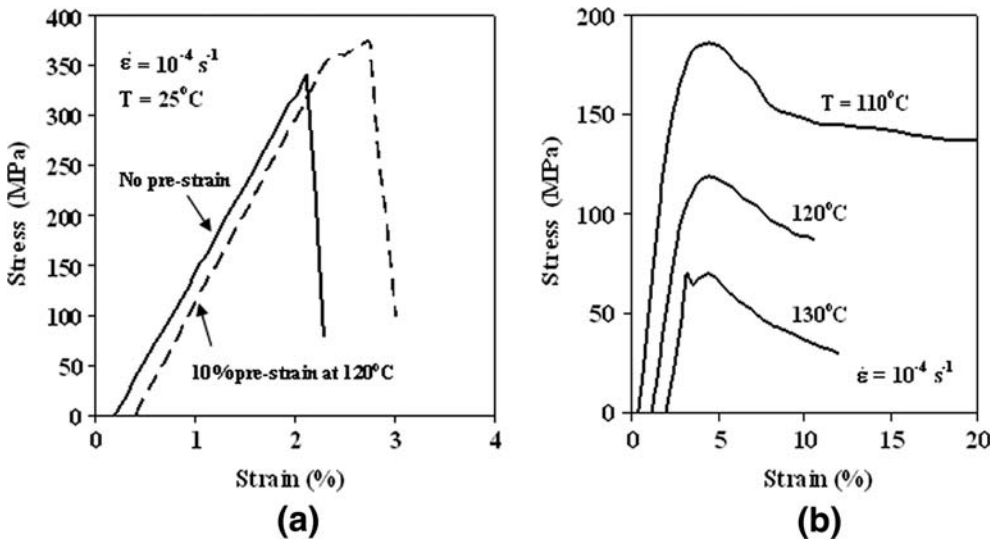

Fig. 8—Stress-strain curves of an amorphous alloy $Ca_{47}Mg_{19}Zn_7Cu_{27}$. Compression tests conducted at (*a*) 25 °C and (*b*) 110 °C, 120 °C, and 130 °C, and a strain rate of 10^{-4} s^{-1}.[11]

VIII. OXIDATION AND CORROSION RESISTANCE

A. *Oxidation Resistance in Air*

The room-temperature oxidation behavior of three Ca-based bulk amorphous alloys, $Ca_{65}Mg_{15}Zn_{20}$, $Ca_{50}Mg_{20}Cu_{30}$, and $Ca_{55}Mg_{18}Zn_{11}Cu_{16}$, was examined under normal flowing laboratory air and compared with the oxidation behaviors of these alloys in crystalline form under identical conditions.[26] The dependences of net mass change due to oxide formation per unit surface area, W, on the oxidation time, t, are presented in Figures 9(a) through (c) for amorphous and crystalline specimens. For each alloy, oxidation occurs at a faster rate in the crystalline condition than in the amorphous condition. In the crystalline $Ca_{65}Mg_{15}Zn_{20}$ and $Ca_{50}Mg_{20}Cu_{30}$ alloys, as well as in the amorphous $Ca_{50}Mg_{20}Cu_{30}$ alloy during the first 600 hours, W increases linearly with t, which can be expressed as follows:

$$W = k_1 t + c_1 \quad [5]$$

On the other hand, oxidation of the crystalline quaternary $Ca_{55}Mg_{18}Zn_{11}Cu_{16}$ alloy, amorphous $Ca_{65}Mg_{15}Zn_{20}$, and $Ca_{55}Mg_{18}Zn_{11}Cu_{16}$ alloys, as well as the amorphous $Ca_{50}Mg_{20}Cu_{30}$ alloy after 600 hours of holding, is better described by a parabolic dependence:

$$W^2 = k_2 t + c_2 \quad [6]$$

In Eqs. [5] and [6], k_1 and k_2 are, respectively, linear and parabolic oxidation-rate constants, and c_1 and c_2 are constants, which reflect the abrupt oxidation of juvenile surfaces during early stages of the oxidation experiment or a change in the mechanism of oxidation (for example, from a linear to a parabolic one). The values of these constants are given in Figure 9 near the corresponding oxidation curves.

The linear time dependence of a specimen mass gain during oxidation (Eq. [5]) is an indication that the rate-determining step for the oxidation reaction is a gas-metal interface reaction.[57,58] This situation generally occurs when the surface oxide has a volume much different than the volume of the alloy from which it forms, and, therefore, it is unable to form a continuous passive layer and suppress further oxidation of the substrate alloy. On the other hand, a parabolic time dependence of the specimen mass gain during oxidation, leading to a decrease in the oxidation rate with time, is an indication that diffusion through the oxide layer becomes the rate-controlling process.[58] This situation generally occurs when the surface oxide has a similar volume as the volume of the alloy participating in the reaction and a passive oxide layer is formed with time. The BMGs usually follow this oxidation-rate law.[57–61] These results show that the $Ca_{55}Mg_{18}Zn_{11}Cu_{16}$ BMG possesses the most favorable oxidation resistance, followed closely by the $Ca_{50}Mg_{20}Cu_{30}$ BMG, with the $Ca_{65}Mg_{15}Zn_{20}$ BMG having the least favorable oxidation resistance. This trend in oxidation resistance follows the same trend as the glass-forming abilities of these three compositions.

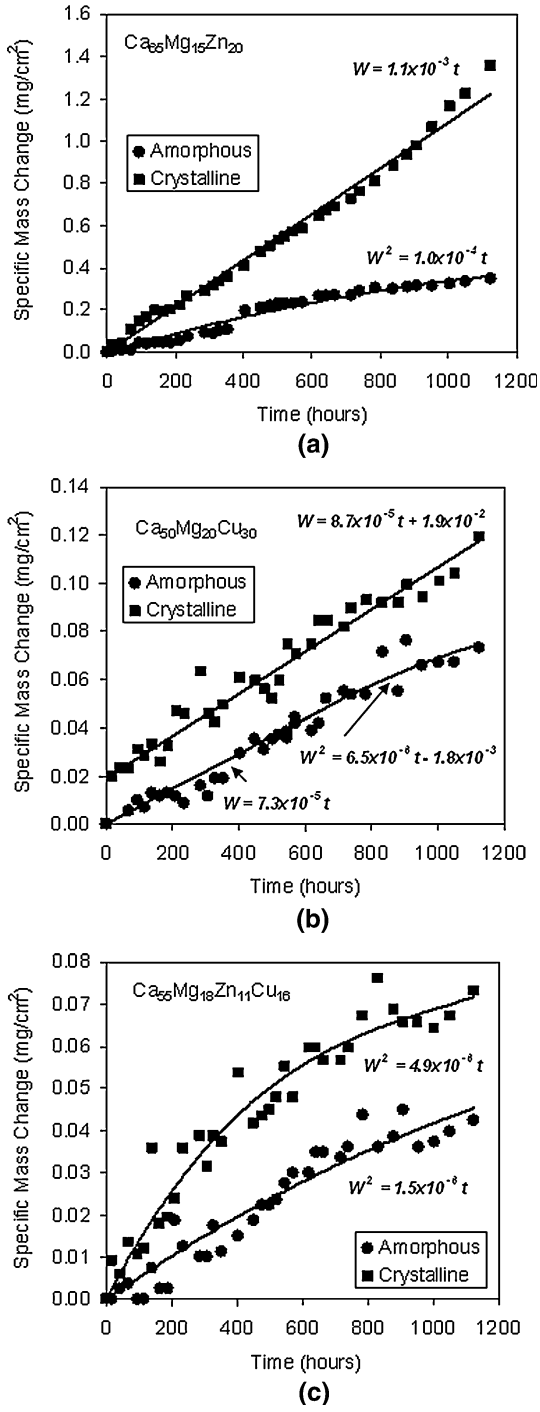

Fig. 9—Specific mass change *vs* holding time in air at room temperature of crystalline and amorphous alloys: (*a*) $Ca_{65}Mg_{15}Zn_{20}$, (*b*) $Ca_{50}Mg_{20}Cu_{30}$, and (*c*) $Ca_{55}Mg_{18}Zn_{11}Cu_{16}$.[26]

B. *Corrosion Resistance in Water*

The corrosion properties of ternary ($Ca_{65}Mg_{15}Zn_{20}$ and $Ca_{50}Mg_{20}Cu_{30}$), quaternary ($Ca_{55}Mg_{18}Zn_{11}Cu_{16}$), and quinternary ($Ca_{55}Mg_{15}Al_{10}Zn_{15}Cu_5$) amorphous alloys were studied using static aqueous submersion at room temperature.[62] The results are shown in Figure 10. Ternary Ca-Mg-Zn and Ca-Mg-Cu BMGs experienced destructive corrosion reactions, resulting

in a net loss of mass from the samples due to spallation of the corrosion products. The weight loss of $Ca_{65}Mg_{15}Zn_{20}$ BMG occurred immediately after immersion in water, but the rate of the weight loss continuously decreased with time, reached a minimum after about 400 hours of holding, and then suddenly increased again, leading to a second cycle of corrosion that was similar to the first cycle; after ~700 hours of holding in water, the sample lost about 65 pct of its mass (Figure 10(a)). X-ray analysis of the spalled corrosion powder product from the $Ca_{65}Mg_{15}Zn_{20}$ amorphous sample identified three primary phases: calcium hydroxide ($Ca(OH)_2$), calcium zinc hydroxide hydrate ($Ca[Zn(OH)_3]_2{\cdot}H_2O$), and calcium zinc ($Ca_3Zn$).

Corrosion behavior of the ternary $Ca_{50}Mg_{20}Cu_{30}$ glassy alloy was considerably different from that of $Ca_{65}Mg_{15}Zn_{20}$ (Figure 10(a)). During the first 100 hours of distilled water exposure, the $Ca_{50}Mg_{20}Cu_{30}$ amorphous alloy showed a very minor weight gain due to the creation of an oxide layer. After this time, the alloy started to lose weight and black spalled material appeared at the bottom of the beaker. After ~150 hours of distilled water exposure, the nonprotective reaction product and the corrosion layer visible on the specimen changed in color from black to a blend of gold and black and a rapid decrease in mass was observed. After about 550 hours of exposure, rapid drops in the sample weight occurred, leading to complete decomposition of the sample (Figure 10(a)). X-ray diffraction of the spalled corrosion product from the $Ca_{50}Mg_{20}Cu_{30}$ amorphous sample showed the presence of two primary phases, Cu_2O and $Ca(OH)_2$, and several minor unidentified phases.

Contrasting the heavy corrosion of the pair of the ternary alloys, both the quaternary ($Ca_{55}Mg_{18}Zn_{11}Cu_{16}$) and the quinternary ($Ca_{55}Mg_{15}Al_{10}Zn_{15}Cu_5$) amorphous alloys demonstrated much better corrosion behavior, steadily gaining weight (Figure 10(b)). The weight gain followed a parabolic dependence with corrosion time, indicating formation of a passive oxide layer on the surfaces. The quaternary alloy gained more weight than the quinternary alloy, which was due to the faster corrosion rate in the former. Scanning electron microscopy analysis showed[62] that, after corrosion in water for ~2100 hours, oxide films of thicknesses ~18 to 23 μm and ~7 to 11 μm were formed on the surfaces of, respectively, $Ca_{55}Mg_{18}Zn_{11}Cu_{16}$ and $Ca_{55}Mg_{15}Al_{10}Zn_{15}Cu_5$ BMGs.

The results of this work indicate that the corrosion resistance of Ca-based BMGs can be considerably improved by combined alloying with Zn and Cu or alloying with Al. The alloy containing Al had the best corrosion resistance in water. Recent studies indicate that Al-containing Ca-based metallic glasses also have superior oxidation resistance in both dry and humid air.[63]

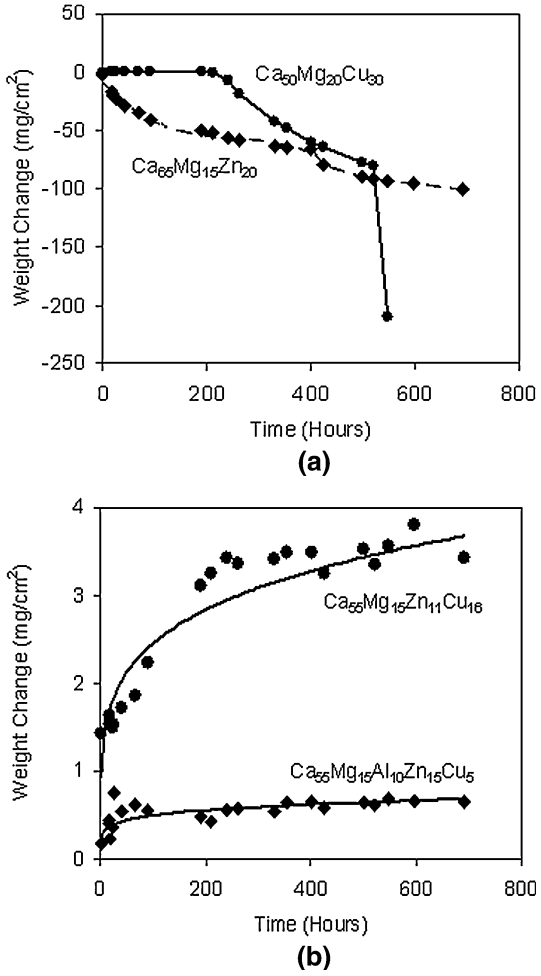

Fig. 10—Mass change per unit area during corrosion in distilled water of the Ca-based BMGs: (*a*) $Ca_{65}Mg_{15}Zn_{20}$ and $Ca_{50}Mg_{20}Cu_{30}$; and (*b*) $Ca_{55}Mg_{18}Zn_{11}Cu_{16}$ and $Ca_{55}Mg_{15}Al_{10}Zn_{15}Cu_5$.[62]

C. *Electrochemical Corrosion*

In recent work, electrochemical behavior in a 0.05 M Na_2SO_4 electrolyte of three Ca-based BMGs, $Ca_{65}Mg_{15}Zn_{20}$, $Ca_{50}Mg_{20}Cu_{30}$, and $Ca_{55}Mg_{18}Zn_{11}Cu_{16}$, has been examined and compared to a crystalline, Mg-based alloy.[64] The cyclic-anodic-polarization curves for these Ca-based BMG alloys and a Mg alloy

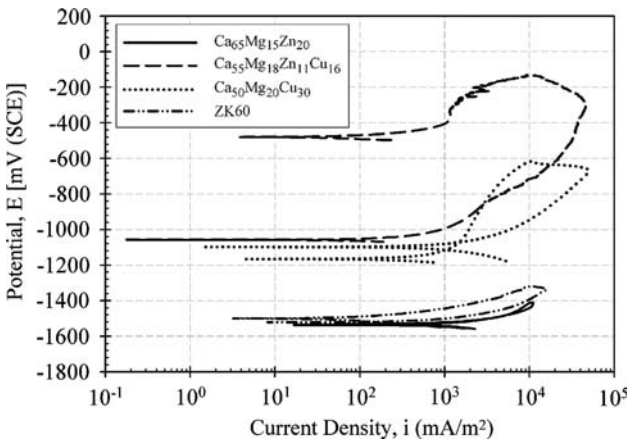

Fig. 11—The average cyclic-anodic-polarization curves for the $Ca_{65}Mg_{15}Zn_{20}$, $Ca_{55}Mg_{18}Zn_{11}Cu_{16}$, and $Ca_{50}Mg_{20}Cu_{30}$ BMG alloys, and the crystalline, Mg-based ZK60 alloy ($Mg_{97.6}Zn_{2.2}Zr_{0.2}$) tested in 0.05 M Na_2SO_4.[64]

ZK60 are plotted in Figure 11. These curves show that $Ca_{65}Mg_{15}Zn_{20}$ and ZK60 Mg were active, $Ca_{55}Mg_{18}Zn_{11}Cu_{16}$ exhibited slight passivity, and $Ca_{50}Mg_{20}Cu_{30}$ was passive at the open-circuit corrosion potential (E_{corr}), with high open-circuit corrosion current densities. The mean corrosion penetration rates (CPRs) for these materials were (a) 5691 ± 1046 μm/year for $Ca_{65}Mg_{15}Zn_{20}$, (b) 311 ± 184 μm/year for $Ca_{55}Mg_{18}Zn_{11}Cu_{16}$, (c) 1503 ± 435 μm/year for $Ca_{50}Mg_{20}Cu_{30}$, and (d) 425 ± 321 μm/year for ZK60. For comparison, a Zr-based BMG alloy Vit105 ($Zr_{52.5}Cu_{17.9}Ni_{14.6}Al_{10}Ti_5$) in a similar 0.05 M Na_2SO_4 electrolyte showed CPR of 0.4 μm/year,[65] an Fe-based BMG in a 0.5 M Na_2SO_4 electrolyte had a CPR of 927 μm/year,[66] and pure Mg in a 0.01 M Na_2SO_4 electrolyte had ~1000 μm/year.[67] Based upon all of these comparisons, it seems that the electrochemical corrosion resistances of Ca-Mg-Zn-Cu and Ca-Mg-Cu glassy alloys are comparable to some Fe-based BMGs and Mg-based crystalline alloys. On the contrary, none of these Ca-based BMGs are as corrosion resistant as the Zr-based BMG alloys.

IX. SUMMARY AND CONCLUSIONS

A new class of BMGs, Ca-based BMGs, has recently been developed. These glasses have the lowest density among all currently known BMGs, and they are built on one or two simple metals, Ca and Mg, while all other BMGs are transition-metal–based alloys. Topological/structural analysis of Ca-based BMGs has shown that they consist of topologically compatible elements, whose atomic size-concentration arrangements provide most efficient atomic cluster packing and lead to a reduced specific volume and a lower free energy. This topological stabilization is one factor contributing to the good GFA and glass stability of Ca-based amorphous alloys. Other contributing factors include low onset driving forces for crystallization of competing crystal phases and high viscosity/relaxation time of the supercooled liquid in these alloys. As these properties depend on alloy composition, the GFA of these glasses is very sensitive to small compositional changes.

The Ca-based BMGs have low elastic moduli and Poisson's ratio. The Young's modulus is ~25 to 35 GPa, shear modulus is ~9 to 13 GPa, and Poisson's ratio is ~0.30 to 0.31. The elastic moduli increase and Poisson's ratio decreases with a decrease in the temperature from T_g to 0 K. The heat capacity of Ca-based BMGs also decreases with a decrease in temperature. The temperature dependence of heat capacity is a combination of the electron contribution (near 0 K), the Debye phonon contribution, and an Einstein harmonic oscillator. The contribution of the latter depends on the alloy composition and decreases with an increase in the fraction of covalent bonding.

The Ca-based BMGs have improved oxidation and corrosion resistance relative to their crystalline counterparts. These properties depend on the composition in such a way that Ca-Mg-Zn glasses have the worst and the Ca-based glasses containing Al have the best resistance to oxidation and corrosion. Optimization of the alloy composition is required to obtain a better combination of required properties.

ACKNOWLEDGMENTS

The authors acknowledge their co-workers, J.M. Scott, J. Dahlman, S. Gorsse, B. Barnard, M. Morrison, and Z. Zhang. Work at the Air Force Research Laboratory and UES, Inc. was supported through Air Force Research Laboratory on-site Contract No. FA8650-04-D-5233 and AFOSR Task No. 01ML05-COR (Dr. J. Fuller, Program Manager). Work at the University of Tennessee was supported through National Science Foundation Grant Nos. DMR-0506292, DMR-0231320 (Mr. C. Huber, Program Director), and DGE-9987548 (Dr. C.J. Van Hartesveldt, Program Director).

REFERENCES

1. A. Inoue: *Acta Mater.*, 2000, vol. 48, pp. 279–306.
2. W.L. Johnson: *MRS Bull.*, 1999, vol. 24, pp. 42–56.
3. W.H. Wang, C. Dong, and C.H. Shek: *Mater. Sci. Eng. Rep.*, 2004, vol. R44, pp. 45–89.
4. O.N. Senkov and J.M. Scott: *Scripta Mater.*, 2004, vol. 50, pp. 449–52.
5. K. Amiya and A. Inoue: *Mater. Trans. JIM*, 2002, vol. 43, pp. 81–84.
6. K. Amiya and A. Inoue: *Mater. Trans. JIM*, 2002, vol. 43, pp. 2578–81.
7. O.N. Senkov and J.M. Scott: *MRS Proc.*, 2003, vol. 806, pp. 145–50.
8. O.N. Senkov and J.M. Scott: *Mater. Lett.*, 2004, vol. 58, pp. 1375–78.
9. O.N. Senkov and J.M. Scott: *J. Non-Cryst. Solids*, 2005, vol. 351, pp. 3087–94.
10. O.N. Senkov and D.B. Miracle: in *Processing and Fabrication of Advanced Materials XIV*, T.S. Srivatsan, R.A. Varin, R. Abbaschian, and S. Viswanathan, eds., ASM INTERNATIONAL, Pittsburgh, PA, 2005, pp. 249–66.
11. O.N. Senkov, D.B. Miracle, and J.M. Scott: *Intermetallics*, 2006, vol. 14, pp. 1055–1160.
12. O.N. Senkov, J.M. Scott, and D.B. Miracle: *J. Alloys Compd.*, 2006, vol. 424, pp. 394–99.
13. E.S. Park and D.H. Kim: *J. Mater. Res.*, 2004, vol. 19, pp. 685–88.
14. E.S. Park, W.T. Kim, and D.H. Kim: *Mater. Sci. Forum*, 2005, vols. 475–479, pp. 3415–18.
15. F.Q. Guo, S.J. Poon, and G.J. Shiflet: *Appl. Phys. Let.*, 2004, vol. 84, pp. 37–39.
16. O.N. Senkov and D.B. Miracle: *Mater. Res. Bull.*, 2001, vol. 36, pp. 2183–98.
17. D.B. Miracle, W. Sanders, and O.N. Senkov: *Phil. Mag. A*, 2003, vol. 83, pp. 2409–28.
18. O.N. Senkov and D.B. Miracle: *J. Non-Crystalline Solids*, 2003, vol. 317, pp. 34–39.
19. O.N. Senkov, D.B. Miracle, and S. Rao: *MRS Proc.*, 2003, vol. 754, pp. 59–64.
20. O.N. Senkov, D.B. Miracle, and H.M. Mullens: *J. Appl. Phys.*, 2005, vol. 97, pp. 103502-1–103502-7.
21. D.B. Miracle: *Nat. Mater.*, 2004, vol. 3, pp. 697–702.
22. D.B. Miracle: *Acta Mater.*, 2006, vol. 54, pp. 4317–36.
23. A. Takeuchi and A. Inoue: *Mater. Trans. JIM*, 2005, vol. 46, pp. 2817–29.

24. V. Keppens, Z. Zhang, O.N. Senkov, and D.B. Miracle: *Phil. Mag*., 2007, vol. 87, pp. 503–08.
25. Z. Zhang, V. Keppens, O.N. Senkov, and D.B. Miracle: *Mater. Sci. Eng. A*, 2007, vol. 471, pp. 151–54.
26. B.R. Barnard, P.K. Liaw, R.A. Buchanan, O.N. Senkov, and D.B. Miracle: *Mater. Trans. JIM*, 2007, vol. 48, pp. 1870–78.
27. *Handbook of Ternary Alloy Phase Diagrams*, P. Villars, A. Prince, and H. Okamoto, eds., ASM INTERNATIONAL, Materials Park, OH, 1995, p. 7522.
28. K.M. Myles: *J. Less-Common Met*., 1970, vol. 20, pp. 149–54.
29. PANDAT, Version 5.0, CompuTherm LLC, Madison, WI 53719.
30. O.N. Senkov, J.M. Scott, and D.B. Miracle: *Mater. Trans. JIM*, 2007, vol. 48, pp. 1610–16.
31. O.N. Senkov, J.M. Scott, and D.B. Miracle: *Metall. Mater. Trans. A*, 2007, vol. 38A, pp. 0000–00.
32. S. Gorsse, G. Orveillon, O.N. Senkov, and D.B. Miracle: *Phys. Rev. B*, 2006, vol. 73, pp. 224202-1–224202-9.
33. C.O. Brubaker and Z.-K. Liu: *J. Alloys Compd.*, 2004, vol. 370, pp. 114–22.
34. L. Kaufman and H. Bernstein: *Computer Calculation of Phase Diagrams*, Academic Press, New York, NY, 1970.
35. D. Kim, B.J. Lee, and N.J. Kim: *Intermetallics*, 2004, vol. 12, pp. 1103–07.
36. D. Kim, B.-J. Lee, and N.J. Kim: *Scripta Mater*., 2003, vol. 52, pp. 969–72.
37. G.W. Scherer: *Relaxation in Glass and Composites*, Wiley-Interscience, New York, NY, 1986.
38. D.B. Dingwell and S. Webb: *Eur. J. Mineral*., 1990, vol. 2, pp. 427–49.
39. C.A. Angell: *Science*, 1995, vol. 267, pp. 1924–26.
40. R. Bohmer, K.L. Ngai, C.A. Angell, and D.J. Plazek: *J. Chem. Phys*., 1993, vol. 99, pp. 4201–09.
41. L. Shadowspeaker and R. Busch: *Appl. Phys. Lett*., 2004, vol. 85, pp. 2508–10.
42. R. Busch, E. Bakke, and W.L. Johnson: *Acta Mater*., 1998, vol. 46, pp. 4725–32.
43. R. Busch, W. Liu, and W.L. Johnson: *J. Appl. Phys*., 1998, vol. 83, pp. 4134–41.
44. M.B. Tang, H.Y. Bai, and W.H. Wang: *Phys. Rev. B*, 2005, vol. 72, pp. 012202-1–012202-4.
45. M.B. Tang *et al*.: *Appl. Phys. Lett*., 2005, vol. 86, pp. 021910-1–021910-3.
46. A.D. Caplin, G. Grüner, and J.B. Dunlop: *Phys. Rev. Lett*., 1973, vol. 30, pp. 1138–40.
47. D. Mandrus, B.C. Sales, and R. Jin: *Phys. Rev. B*, 2001, vol. 64, pp. 012302-1–012302-4.
48. V. Keppens *et al*.: *Nature*, 1998, vol. 395, pp. 876–78.
49. S.F. Pugh: *Philos. Mag*., 1950, vol. 45, pp. 823–28.
50. J.J. Lewandowski, W.H. Wang, and A.L. Greer: *Philos. Mag. Lett*., 2005, vol. 85, pp. 77–87.
51. J. Schroers and W.L. Johnson: *Phys. Rev. Lett*., 2004, vol. 93, pp. 255506-1–255506-4.
52. X.J. Gu, A.G. McDermott, S.J. Poon, and G.J. Shiflet: *Appl. Phys. Lett*., 2006, vol. 88, pp. 21905-1–21905-3.
53. F. Spaepen: *Acta Metall*., 1977, vol. 25, pp. 407–15.
54. L.A. Davis: *Metallic Glasses*, ASM International, Materials Park, OH, 1978, pp. 191–223.
55. T. Masumoto and R. Maddin: *Mater. Sci. Eng*., 1975, vol. 19, pp. 1–24.
56. F. Spaepen and A.I. Taub: in *Amorphous Metallic Alloys*, F.E. Luborsky, ed., Butterworth and Co., London, 1983, pp. 231–56.
57. W. Kai, H.H. Hsieh, T.G. Nieh, and Y. Kawamura: *Intermetallics*, 2002, vol. 10, pp. 1265–70.
58. J.M. West: *Basic Corrosion and Oxidation*, Ellis Horwood, West Sussex, England, 1980.
59. L. Liu and K.C. Chan: *Appl. Phys. A*, 2005, vol. 80, pp. 1737–44.
60. A. Dhawan, K. Raetzke, F. Faupel, and S.K. Sharma: *Phys. Status Solidi A*, 2003, vol. 199, pp. 431–38.
61. X. Sun, S. Schneider, U. Geyer, W.L. Johnson, and M.-A. Nicolet: *J. Mater. Res*., 1996, vol. 11, pp. 2738–43.
62. J. Dahlman, O.N. Senkov, J.M. Scott, and D.B. Miracle: *Mater. Trans. JIM*, 2007, vol. 48, pp. 1850–54.
63. J. Dahlman, O.N. Senkov, J.M. Scott, and D.B. Miracle: unpublished work, Air Force Research Laboratory, Wright-Patterson AFB, 2007.
64. M.L. Morrison, R.A. Buchanan, O.N. Senkov, D.B. Miracle, and P.K. Liaw: *Metall. Mater. Trans. A*, 2006, vol. 37A, pp. 1239–45.
65. W.H. Peter *et al*.: *Intermetallics*, 2002, vol. 10, pp. 1157–62.
66. D. Szewieczek, and A. Baron: *J. Mater. Proc. Technol*., 2005, vols. 164–165, pp. 940–46.
67. G. Baril and N. Pebere: *Corr. Sci*., 2001, vol. 43, pp. 471–84.